



# Kent Academic Repository

Njogu, Peter M., Sanz-Izquierdo, Benito, Jun, Sung Yun, Kalman, Gabriel, Gao, Steven, Malas, Asish and Gibbons, Gregory J. (2020) *Evaluation of Planar Inkjet-Printed Antennas on a Low-Cost Origami Flapping Robot*. IEEE Access, 8 . pp. 164103-164113.

## Downloaded from

<https://kar.kent.ac.uk/85595/> The University of Kent's Academic Repository KAR

## The version of record is available from

<https://doi.org/10.1109/ACCESS.2020.3020824>

## This document version

Publisher pdf

## DOI for this version

## Licence for this version

CC BY (Attribution)

## Additional information

## Versions of research works

### Versions of Record

If this version is the version of record, it is the same as the published version available on the publisher's web site. Cite as the published version.

### Author Accepted Manuscripts

If this document is identified as the Author Accepted Manuscript it is the version after peer review but before type setting, copy editing or publisher branding. Cite as Surname, Initial. (Year) 'Title of article'. To be published in *Title of Journal*, Volume and issue numbers [peer-reviewed accepted version]. Available at: DOI or URL (Accessed: date).

## Enquiries

If you have questions about this document contact [ResearchSupport@kent.ac.uk](mailto:ResearchSupport@kent.ac.uk). Please include the URL of the record in KAR. If you believe that your, or a third party's rights have been compromised through this document please see our [Take Down policy](https://www.kent.ac.uk/guides/kar-the-kent-academic-repository#policies) (available from <https://www.kent.ac.uk/guides/kar-the-kent-academic-repository#policies>).

Received August 10, 2020, accepted August 20, 2020, date of publication September 1, 2020, date of current version September 21, 2020.

Digital Object Identifier 10.1109/ACCESS.2020.3020824

# Evaluation of Planar Inkjet-Printed Antennas on a Low-Cost Origami Flapping Robot

PETER M. NJOGU<sup>1</sup>, BENITO SANZ-IZQUIERDO<sup>1</sup>, (Member, IEEE),  
SUNG YUN JUN<sup>2</sup>, (Member, IEEE), GABRIEL KALMAN<sup>3</sup>,  
STEVEN GAO<sup>1</sup>, (Fellow, IEEE), ASISH MALAS<sup>4</sup>,  
AND GREGORY J. GIBBONS<sup>5</sup>

<sup>1</sup>School of Engineering and Digital Arts, University of Kent, Canterbury CT2 7NZ, U.K.

<sup>2</sup>RF Technology Division, National Institute of Standards and Technology, Boulder, CO 80305, USA

<sup>3</sup>CommScope Technologies U.K., MWS/IS European Engineering, Kirkcaldy KY2 6NA, U.K.

<sup>4</sup>PolyMERIC Innovation Centre, London South Bank University, TWI Ltd., Cambridge, U.K.

<sup>5</sup>Additive Manufacturing Group, WMG, The University of Warwick, Coventry CV4 7AL, U.K.

Corresponding author: Benito Sanz-Izquierdo (b.sanz@kent.ac.uk)

This work was supported in part by the U.K. Engineering and Physical Sciences Research Council (EPSRC) through the High Value Manufacture Fellowship (HVMC) under Grant EP/L017121/1, through the WISDOM Project within the CHIST ERA under EPSRC Grant EP/P015840/1, and through the Low-Profile Ultra-Wideband Wide-Scanning Multi-Function Beam-Steerable Array Antennas Project under Grant EP/S005625/1; and in part by the Royal Society International Exchanges 2019 Cost Share (NSFC) under Grant IEC\NSFC\191780.

**ABSTRACT** An investigation on antenna solutions for expendable origami paper flapping robots is presented. An origami flapping robotic bird that can be produced using standard A4 paper is employed. Antennas resonating at the two commonly used frequency bands, 2.4 GHz and 5.2 GHz, are designed for the limited space available on the folded origami structure. Two developments of the same dual-band monopole antenna are discussed. The first antenna is located on the robot's spine and the second on its tail. A space diversity configuration is also studied. The antennas are printed directly onto a photo paper substrate and then folded into an origami robotic crane's body structure. An ordinary desktop inkjet printer fitted with silver nanoparticle conductive ink cartridges has been employed. CST Microwave Studio<sup>TM</sup> has been used to design the antennas. A good agreement between the measured and simulated  $S_{11}$  results is achieved with a reasonable  $-10\text{dB}$  impedance bandwidth realized in the three cases studied. The radiation patterns are omnidirectional in the XZ plane which is desirable for the specific application. The diversity configuration has a mutual coupling of  $< -23\text{dB}$  and a gain of 1.4 dB and 2.8 dB at 2.4 GHz and 5.2 GHz respectively. The aim is to provide a new vision for antennas embedded into expandable flying robots based on traditional origami structures.

**INDEX TERMS** Inkjet printing, origami, 3D printing, antennas, drone, coplanar waveguide (CPW), CST.

## I. INTRODUCTION

Small robots have attracted interest from both academic and industrial world in recent years. This seems to be driven by the increasing miniaturisation of mechanical, electrical and electronic components [1], [2]. Different types of small robots have been developed including remote controlled vehicles [3] and flying robots [4], [5]. Origami foldable robots have also stirred researchers' interests and have been studied from various perspectives [6]. This is driven by the unique ways of fabricating and assembling of various types of origami inspired structures [7]. Among origami

inspired applications are electronic components [8] and robots [9].

Flying robots are used by military, security, civil and commercial applications in areas such as correction and relaying of real-time data of an occurrence. They enable effective responses in areas like disaster zones, farming, reconnaissance, environmental observation and monitoring, meteorological observation and research, and mineral exploitation etc. [10]–[12].

Key for swift and flexible mobility controllability and operation of flying robots is the wireless communications for which antennas are an essential element. A firm, compact, low profile aerodynamic enhancing antenna mounted on a robot facilitates reliable drone-controller communication.

The associate editor coordinating the review of this manuscript and approving it for publication was Jaime Laviada<sup>1</sup>.

In most cases, this antenna should provide omnidirectional radiation pattern and vertical polarisation for efficient communication with the controller [13].

3D inkjet printing with nanoparticle silver ink is a rapidly advancing manufacturing method. It is a layer by layer fabrication process where a design can be printed directly from a digital model. It offers rapid prototyping and can reduce manufacturing process cycles in areas such as electronics, microwave and radio frequency (RF) [14].

Inkjet printing has been employed in the development of antennas on various substrate such as 3D printed polylactic acid (PLA) [15], [16] thermoplastic acrylonitrile butadiene styrene polycarbonate (ABS-PC) [17], polyethylene terephthalate (PET) [18], flexible thermoplastic polyurethane (NinjaFlex) [19], textile [20], Rogers RO 3203 [21] etc. Further developments on inkjet printing technology have enabled printing of antennas on paper-based substrates [22]–[27]. Examples include monopole antennas and designs suitable for RFID applications [22], ultra wideband antennas [23]–[25], and fractal geometries based on a triangular Sierpinski concept [26]. Miniaturized MIMO antennas have also been proposed by printing on a Kodak film paper which are then folded on a cylindrical shape [27].

This article investigates the integration of inkjet-printed antenna on a flying robot that is produced using traditional origami techniques. This type of flying robots are gaining popularity in the research and development community [28], [29]. A compact dual-band antenna consisting of a triangular shape with a horizontal slot on top of a semi-elliptical monopole is employed. Low-cost inkjet printing on photo paper substrate is used. It is the first time that a geometry has been developed to specifically fit within the folds of a traditional origami bird folded from an A4 paper sheet. Three positions are found to be suitable for the antenna: triangular neck, spine and tail. Consequently, two versions of the same antenna designs are produced. One fits on the robot’s spine while the other fits on the tail and/or the neck. The latter is further investigated in a diversity configuration.

The rest of the paper is organized as follows: Section ? describes the design and analyses the antenna located on the spine, section ? studies the antenna located on the tail, section ? describes diversity antenna system solution while section ? is the conclusion and discussion.

## II. DESIGN AND ANALYSIS OF THE SPINE ANTENNA

### A. ANTENNA DESIGN ANALYSIS AND GEOMETRY

A traditional flapping origami robot with potential electromechanical and antenna components locations is illustrated in Fig.1. Fig. 2(a) shows the fold lines along which the origami bird is folded from a 210 mm square (about A4 size) sheet. It also shows the location for a spine antenna. The bands targeted for the flying robot application are 2.4 GHz and 5.2 GHz WLAN/WiFi communication bands [30], [31]. The proposed planar monopole antenna (Fig. 2(b)) is based on [32], [33] and its geometry is modelled around [34]. It is a leaf shaped monopole with a semi-elliptical bottom and a

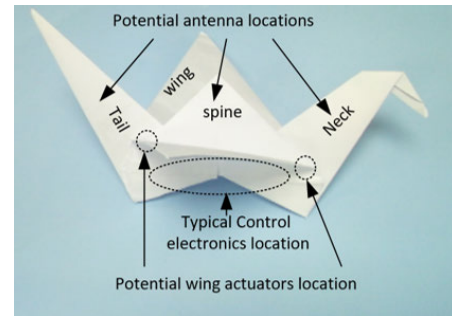


FIGURE 1. The origami robotic bird and potential antenna locations.

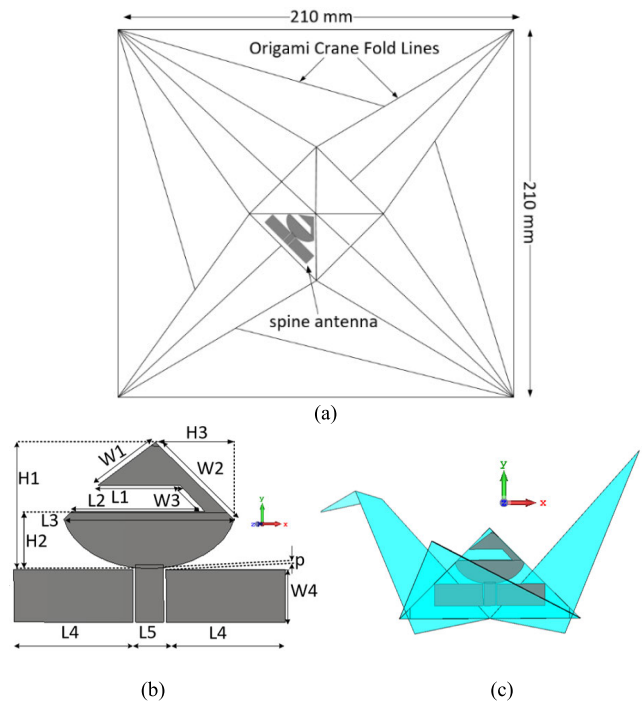


FIGURE 2. Antenna integrated onto the Spine of the origami crane: (a) illustration of the spine antenna in the unfolded robot layout, (b) the optimized antenna and (c) location on robot.

triangular top with a horizontal slot. Its dimensions are given in Table 1. The lower semi-elliptical section fit in the lower wider section of the triangular spine while the triangular upper part fits in its apex as shown in Fig. 2 (c). The antenna orientation is as that of the spine i.e. upright. A 50Ω CPW line feeds the antenna. Two rectangular ground plane are on either sides of the CPW feed line.

The lower frequency ( $f_L$ ) of a planar elliptical disc monopole corresponding to  $VSWR = 2$  is approximated by equating its area to the area of an equivalent cylindrical monopole of the same height  $L$  and equivalent radius  $r$ :

$$2\pi rL = \pi R_1R_2 \tag{1}$$

where  $R_1$  and  $R_2$  are the longer and shorter half lengths of ellipse’s axes respectively. Equation (1) thus gives:

$$r = (R_1R_2)/2L \tag{2}$$

A quarter wavelength monopole antenna has an input impedance equivalent to half of that of a half wavelength

**TABLE 1. Antenna optimum dimensions in millimeters (mm).**

Dimensions	L1	L2	L3	L4	L5	W1	W2
Value (mm)	15.4	25.1	32.2	22.5	5.3	13.6	19
Dimensions	W3	W4	H	R1	R2	p	
Value (mm)	2.2	6.9	24.24	11.75	16.8	0.4	

dipole antenna. The input impedance of an infinitesimally thin monopole antenna is thus  $36.5 + j21.25\Omega$ , an inductive impedance. The real impedance is obtained by using a slightly smaller length,  $L$ , of the monopole given by [35].

$$L = 0.24\lambda F \tag{3}$$

where  $\lambda$  is the free space wavelength and  $F$  is the length-to-radius parameter for the stub monopole given by

$$F = (L/r) / (1 + L/r) = L/L + r \tag{4}$$

From equations (3) and (4), the wavelength  $\lambda$  is obtained as:

$$\lambda = (L + r) / 0.24 \tag{5}$$

Thus the lower frequency  $f_L$  is:

$$f_L = c/\lambda = (30 \times 0.24)/(L + r) = 7.2/(L + r) \tag{6}$$

After accounting for the effect of probe length,  $p$ , which increase the antenna length and thus reducing the frequency, (6) can accordingly be modified to

$$f_L = 7.2/(L + r + p) \tag{7}$$

where  $f_L$  is in GHz and  $L$ ,  $r$  and  $p$  are in cm. For the half lengths axes  $R_1$  and  $R_2$ , the ellipticity ratio,  $R_1/R_2$ , chosen was 1.3 to restrict the bandwidth to the range of interest. The antenna was fed along the minor axis of the semi ellipse. For elliptical monopole fed along the minor axis,  $L = 2R_2$  and  $r = R_1/4$ . For a  $f_L$  equal to 2.4 GHz, the radii  $R_1$  and  $R_2$  of the semi-ellipse after optimization were obtained.

A planar triangular monopole of height  $H$  (height from feed point to apex) and base length  $W$  was superimposed on the semi elliptical monopole.  $H$  is the height of the equivalent cylindrical monopole of radius  $r$ .  $H$  and  $r$  are calculated from (6), (8) and (10):

$$H = \sqrt{3}W/2 \tag{8}$$

$$r = W/4\pi \tag{9}$$

The actual height  $H$  is less than the calculated height due to dielectric substrate and fringing currents effect. It should be noted that the superimposed rounded triangular monopole base is the semi-elliptical disc.

The model was simulated on a 0.177 mm thick paper substrate of relative permittivity,  $\epsilon_r$ , of 3 using CST Microwave Studio<sup>TM</sup>. Fig. 3 shows the response of the various component of the radiator. The semi elliptical radiator provides a resonant at upper band. The semi-elliptical radiator with superimposed triangular monopole exhibits wide-band characteristics. The lower frequency is higher than the targeted 2.4 GHz. This could be due to the rounded (semi-ellipse) base of the triangular monopole which reduces

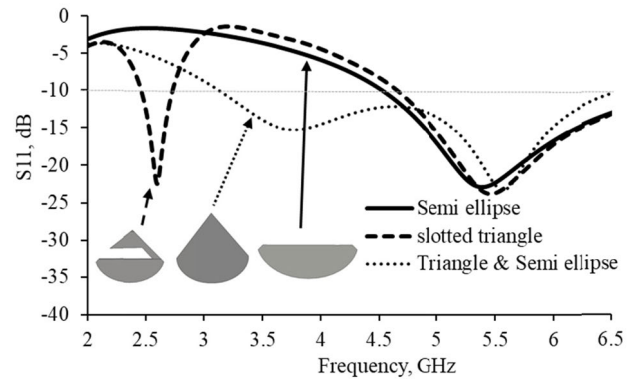


**FIGURE 3. Radiating element configuration for respective resonance.**

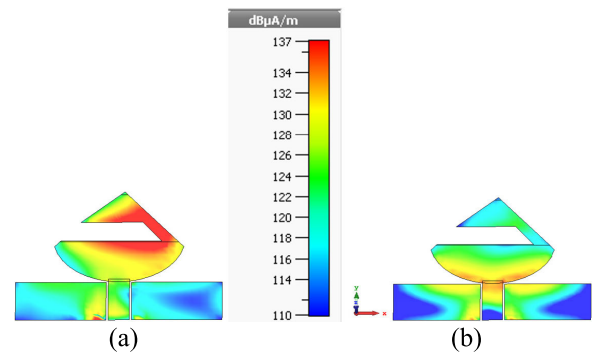


**FIGURE 4. Surface current distribution for spine antenna (a) 2.4 GHz and (b) 5.2 GHz.**

the size of radiator thus raising  $f_L$ . By inserting and optimizing the dimension of a horizontal slot across the triangle, the lower resonance point was shifted to 2.4 GHz while maintaining the upper band as well as rejecting frequencies between the two bands of interest. The final antenna has two distinct resonant modes corresponding to the triangular radiating section and the semi ellipse. The gap ‘ $p$ ’ between the ground plane and radiating acts as a matching network and improves impedance bandwidth. The optimum impedance bandwidth is achieved when the capacitance due to the gap ‘ $p$ ’ between the radiating element and ground plane edges balances with the antenna inductance.

The size of the ground plane is also critical in the design of compact antennas [36], [37]. The surface current distribution on the antenna is shown in Fig. 4. As expected, at 2.4 GHz,

Fig. 4 (a), most of the currents is concentrated in the triangular section. At 5.2 GHz, Fig. 4 (b), most of the currents are in the lower section of the semi-ellipse. As with all compact antennas on small ground planes, some currents are also present on the antenna’s ground elements. These currents are strongest at the upper edges of the rectangular ground planes at 5.2 GHz than at 2.4 GHz. Taking this into consideration, it can be inferred that the surface current distribution could change with the size and the shape of the ground plane and/or with introduction of cable and/or RF connector to the antenna. This is likely to introduce differences in the measurements in relation to simulations.

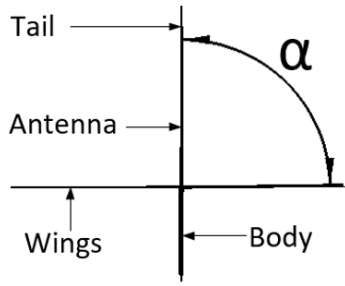


FIGURE 5. Wing angle  $\alpha$  relative to the wings horizontal position.

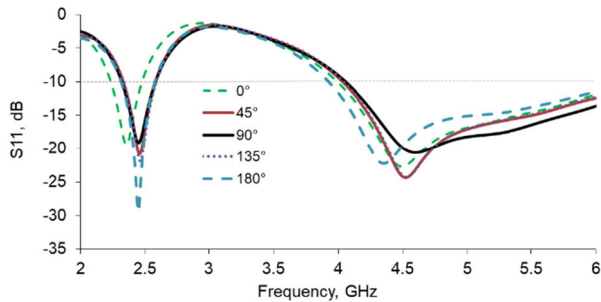


FIGURE 6. Effect of change of angle  $\alpha$  on the reflection coefficient.

### B. INVESTIGATION OF EFFECT WINGS MOVEMENT

The effect on the antenna performance by the wings' flapping during flight was investigated. Fig. 5 depicts the flap angle  $\alpha$  of the wings in relation to vertical core of the bird structure. Fig. 6 shows the simulation reflection coefficients ( $S_{11}$ ) for various values of  $\alpha$ :  $0^\circ$ ,  $45^\circ$ ,  $90^\circ$ ,  $135^\circ$  and  $180^\circ$ . The horizontal position of the wings was defined as the  $90^\circ$  position. The wings extreme upward flap was designated as  $0^\circ$  and the extreme downward as  $180^\circ$ . In the horizontal position,  $-10$  dB impedance bandwidth of the antenna is from 2.3 GHz to about 2.6 GHz at the lower band and from 4 GHz to 6 GHz at the higher band. There is no significant change in  $S_{11}$  from  $1^\circ$  to  $180^\circ$ . Only angles of less than  $1^\circ$  produced an  $S_{11}$  higher than  $-10$  dB at the target 2.4 GHz to 2.5 GHz band. In the worst scenario, at  $0^\circ$ , the  $S_{11}$  was less than  $-8$  dB across the 2.4 GHz band.

### C. SPINE ANTENNA FABRICATION AND MEASUREMENTS

The CST model was exported to Gerber (single layer) and then converted to a PDF file using ViewMate. The PDF was then printed using silver nanoparticles ink that is based on chemical sintering. Chemical sintering technology was used to avoid the prolonged heat sintering and the damage it can cause when the substrate used is a paper based material [38]. In chemical based sintering, a polymer latex and halide emulsion solvent dissolves silver nanoparticles of less than  $0.1 \mu\text{m}$ . Conductivity appears moments after the solution has dried. This makes the ink based on chemical sintering ideal for inkjet printing of the antennas. A  $1200 \times 6000$  dpi resolution and piezo with 210 x3 colour print head home desktop Brother MFC-J5910DW printer was employed. AgIC-AN01 Silver Nano Ink was loaded in the 3 colour

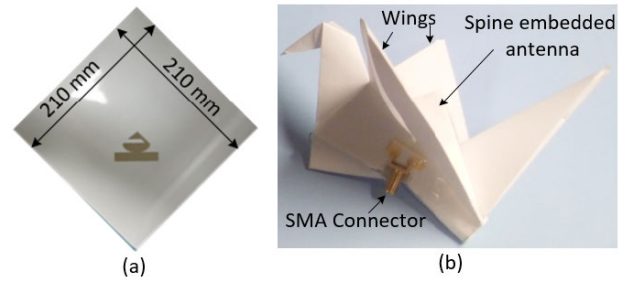


FIGURE 7. (a) Photo paper printed tail antenna folded into a (b) folded into a robotic bird.

cartridges to produce a thick print layer that can achieve sufficient conductivity. The silver ink provides a resistivity of  $0.2 \Omega/\text{sq}$  when printed on an AgIC-CP01A4 photopaper [39]. Further analytical tests on a variety of printed tracks were carried out using the equation for the resistivity,  $\rho$ :

$$\rho = R \frac{A}{l} \quad (10)$$

where  $R$  is the measured resistance,  $A$  is the cross-sectional area and  $l$  is the length of the track. The values of resistivity obtained were between  $2 \times 10^{-7}$  and  $3 \times 10^{-7}$  which is about the same value to the one provided by the manufacturers for a layer thickness of about  $1 \mu\text{m}$ .

The printed antenna is shown in Fig. 7(a). The printout was folded into a robotic bird. The antenna was concealed inside the structure to protect the printed metallic layers from environmental damage as shown in Fig. 7(b) Thermal and mechanical stability of the printed layers were provided by AgIc. Heat resistance can be allowed for up to 30 minutes at  $100^\circ\text{C}$ . In cross cut tests (ISO 2409), the mechanical stability is between 0 to 1 (0 is highest and 5 is lowest).

Surface profiles of the antenna's silver ink were obtained using white light interferometry (profilometer). The images at 50x magnification are shown in Fig. 8(a). An average surface roughness of approximately  $S_a 200\text{nm}$  was obtained. The image shows that the 3D print is not uniform as the substrate can be seen through the silver ink. The droplets are visible and the measured roughness is for both paper substrate and silver droplets. Fig. 8(b) is an optical image of top view of the printed antenna of  $1 \mu\text{m}$  silver ink height taken with x10 magnification which shows uneven surface. Black regions are seen within the sample which could be deeper unevenness of ink surface. Fig. 8(c) shows the narrow gap between CPW and the ground plane taken with x20 magnification for the  $1 \mu\text{m}$  silver ink height. Some isolated silver ink particles can be seen inside the gap but their isolation prevents short circuit across the two parts. The presence of ink particles in the gap does not have any significant effect on the performance of the antennas as the foregoing tests shows. This could be because the particle sizes are much smaller compared to the wavelength of the frequencies involved.

To test the antenna, a 3.5 mm SMA connector was attached to it using Araldite Rapid Epoxy Adhesive. The antenna was concealed inside the structure to protect the printed metallic layers from environmental damage. A Rohde & Schwarz

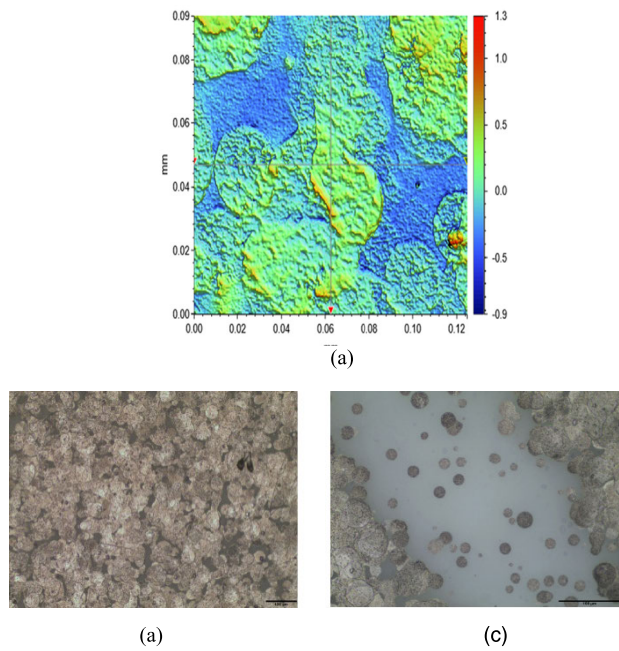


**FIGURE 8.** (a) Silver paint optical interferometry image (b) Silver ink top view optical microscopic image (c) image of the gap between CPW and the ground plane.

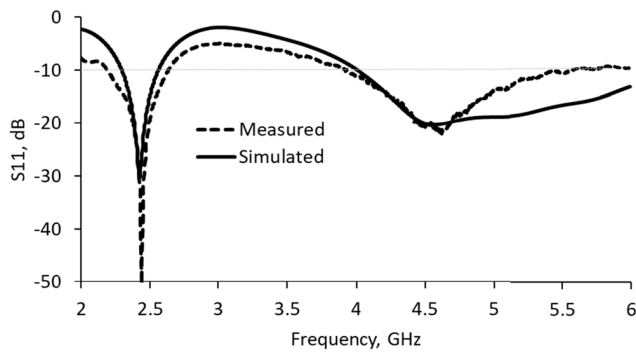


**FIGURE 9.** Measured and simulated  $S_{11}$  compared.

ZVL vector network analyser was used for  $S_{11}$  measurements. Fig. 9 shows the simulated and measured  $S_{11}$  when the wings are horizontal. The measured lower band has  $-10$  dB impedance bandwidth from 2.2 GHz to 2.7 GHz while the upper band has a bandwidth from 3.9 GHz to 5.5 GHz thus covering both target bands. The slight discrepancy between the simulated and the measured  $S_{11}$  could be due to fabrication, folding and measurements errors. These includes non-uniformly deposited silver conductive ink and resistive losses of the printed tracks, the bending of the substrate, as well as the SMA connector.

Fig. 10 shows the simulated and measured radiation patterns at (a) 2.4 GHz and (b) 5.2 GHz for the robot's horizontal wing position i.e.  $\alpha$  is equal to  $90^\circ$ . The simulated results show that as expected for this type of antennas, the planes xy and yz has nulls in the y axis while plane xz displays an omnidirectional pattern. Tests showed no significant effect on the radiation pattern when the position of the wings is varied

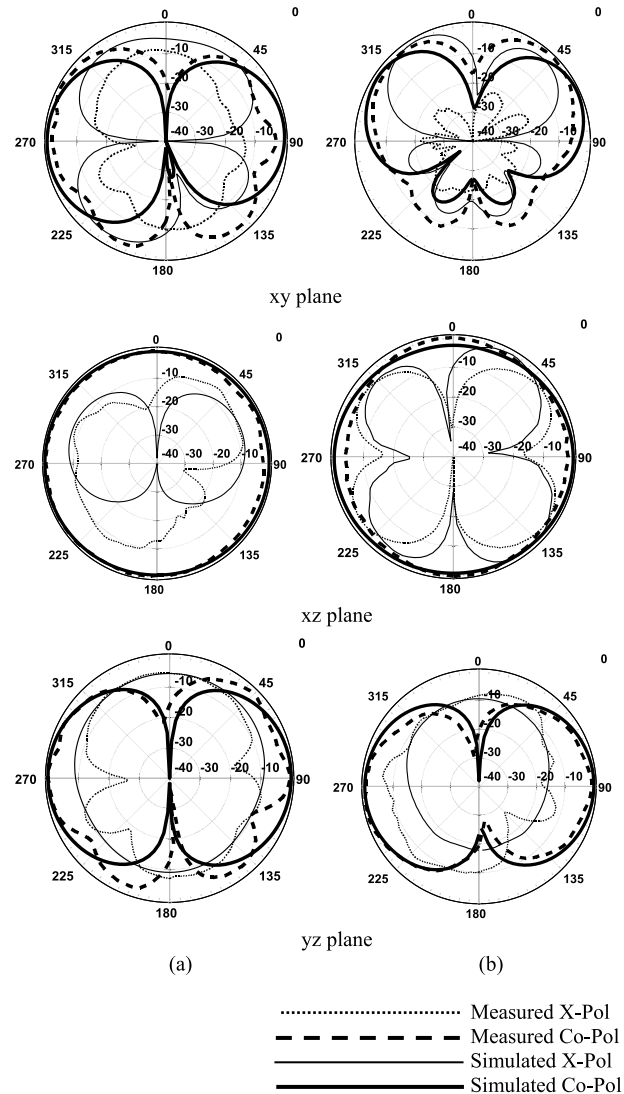


**FIGURE 10.** Simulated and measured radiation pattern for planes xy, xz and yz at (a) 2.4 GHz and (b) 5.2 GHz.

from  $0^\circ$  to  $180^\circ$  relative to the robot's core. The measured antenna radiation patterns are consistent the simulations. As with planar monopoles [40], it exhibits high cross polarization. The high cross polarization component as a result of excitation order modes, radiation due to  $J_x$  current at the top edges of the ground plane near the radiating element. Discontinuity at substrate and metallic radiator results in surface waves adding to cross polarization [41]. Fig. 11 shows the gain vs frequency response for the selected frequency bands. The measured antenna gains were 1.4 dBi and 2.7 dBi at 2.4 GHz and 5.2 GHz respectively, about 0.2 dB and 0.5dB lower than the simulated one. The differences between the simulated and measured gain could be due to fabrication and folding errors, cables and connectors.

### III. A SINGLE CPW-FED TAIL ANTENNA

#### A. TAIL ANTENNA DESIGN

An alternative antenna location is the tail of the origami crane. Fig. 12(a) illustrates the location of a tail antenna

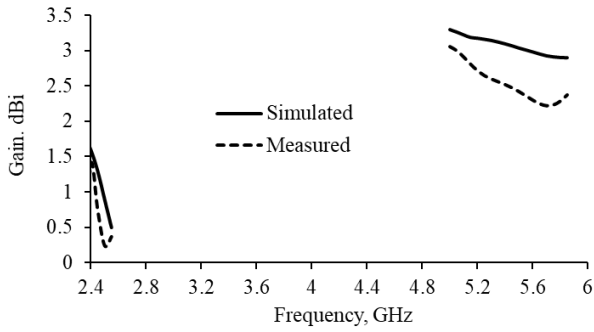


FIGURE 11. Spine antenna gain-frequency response at 2.4 and 5.2 GHz.

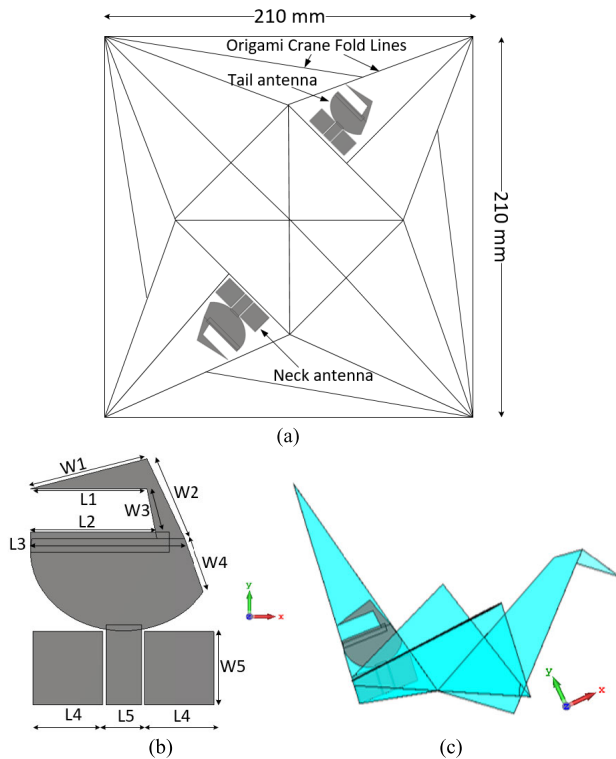


FIGURE 12. Antenna integrated onto the tail of the origami crane: (a) illustrative tail and neck antennas location in the unfolded layout, (b) tail antenna and (c) location on the robot.

as well as the potential symmetrical location for a neck antenna, on 210 by 210 mm unfolded photo paper substrate. Fig. 12 (b) show the antenna’s structure and dimensions while Fig. 12(c) shows its location on the robot’s tail and rotated to fit on the tail’s orientation. Like the previous antenna, the antenna is concealed inside structure to protect the printed metallic layers from environmental damage. The antenna is similar in shape and construction to that described in section IIA with slight dimension adjustments to fit in the narrower tail area and achieve the bandwidths of interest. Table 2 show its final dimensions. The same dielectric material and substrate thickness was used.

The simulated  $S_{11}$  results, Fig. 13, indicates a narrower  $-10$  dB bandwidth at the 2.4 GHz band but a wider  $-10$  dB bandwidth at the 5.2 GHz bands for the angle  $\alpha$  of wing

TABLE 2. Final dimensions of the optimized tail antenna (MM).

L1	L2	L3	L4	L5	W1	W2	W3	W4	W5
17.5	19	23	10.5	5.8	18	13.28	7.65	8.55	11

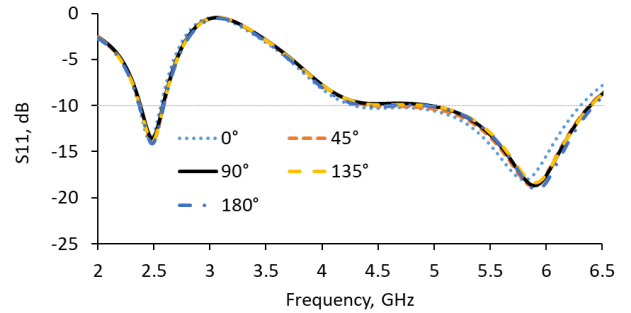


FIGURE 13. Tail antenna simulated  $S_{11}$  for angle  $\alpha$ .

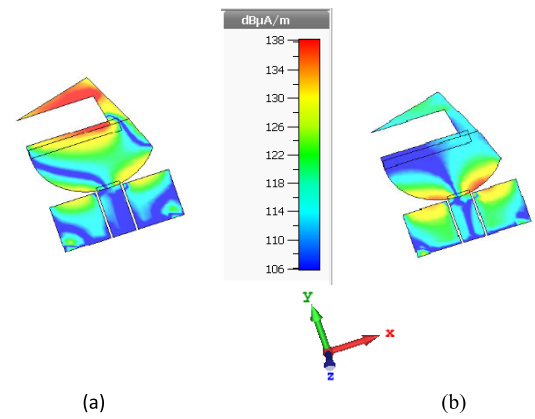


FIGURE 14. Surface current distribution for tail antenna (a) 2.4 GHz and 5.2 GHz.

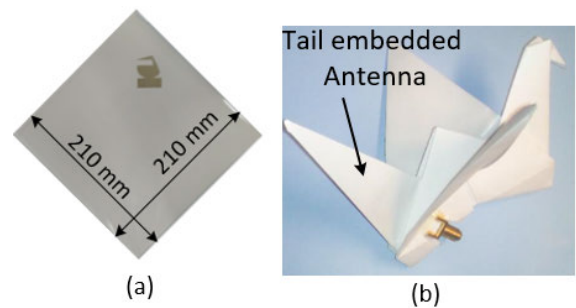


FIGURE 15. (a) Tail antenna printed on a photo paper and (b) folded into a robotic bird.

the flapping. The antenna covers the desired frequency bands for the range of angles of flap. They also show a near negligible effect on  $S_{11}$  by the flapping of the wings. This could be due to the antenna on the tail being removed from the wings bearing section of the origami bird structure. This makes the antenna less obstructed by the flapping of the wings compared to the antenna on the spine (Fig. 7b).

Fig. 14(a) and Fig. 14(b) depicts the surface current distribution at 2.4 GHz and 5.2 GHz respectively. The figure

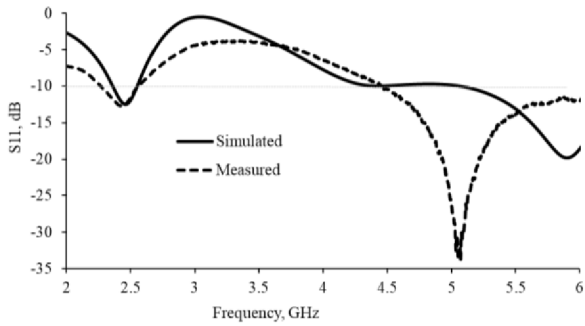


FIGURE 16. Measured vs simulated tail antenna  $S_{11}$ .

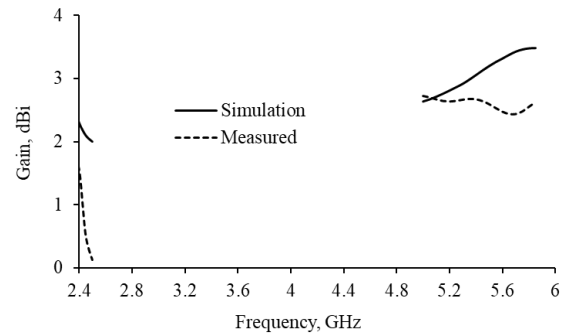


FIGURE 18. Tail antenna gain-frequency response at 2.4 and 5.2 GHz.

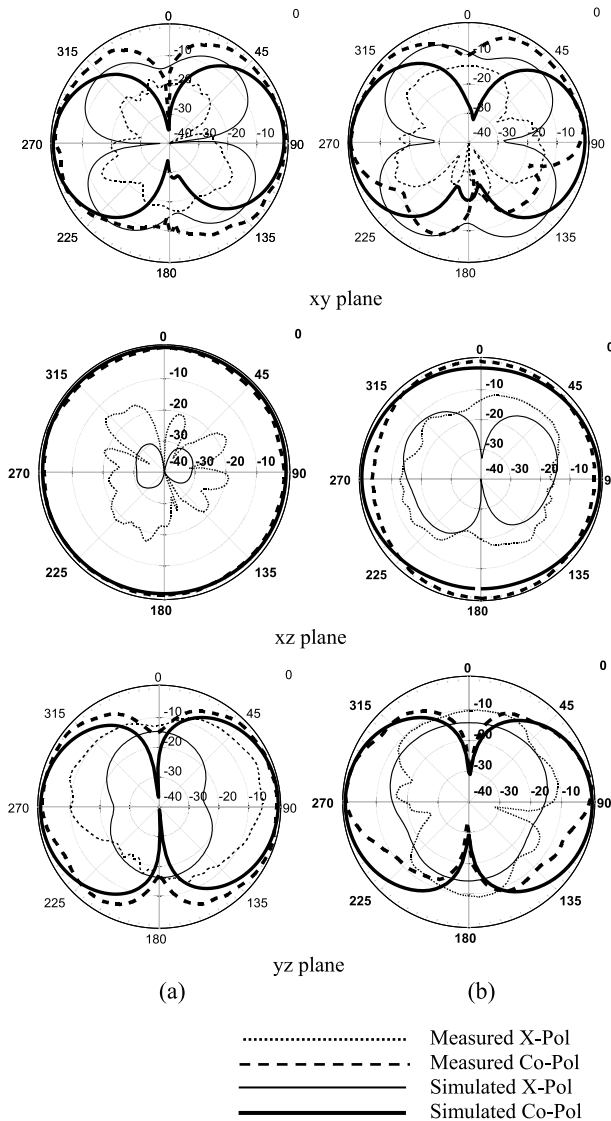


FIGURE 17. Simulated and measured radiation patterns for  $xy$ ,  $xz$ , and  $yz$  planes at (a) 2.4 GHz and (b) 5.2 GHz.

indicates a high level of surface current at the triangular and rounded sections of the antenna at 2.4 GHz and 5.2 GHz resonance points respectively. A high surface current level is also observed on the ground plane at the two bands due to its small size which makes it a sensitive part of the radiating structure [37].

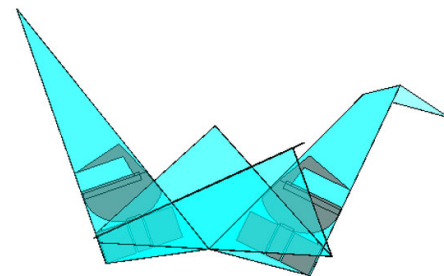


FIGURE 19. Simulated neck diversity antenna.

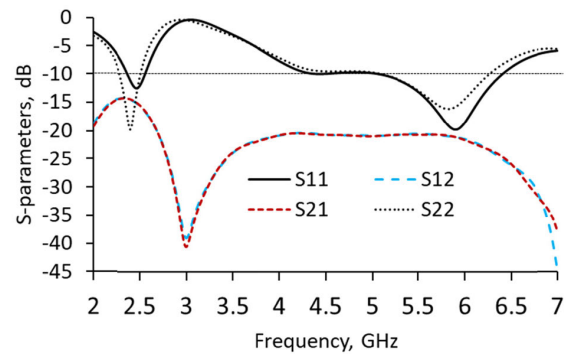


FIGURE 20. Simulated diversity antennas  $S$ -parameters.

### B. FABRICATION AND MEASUREMENTS

The fabrication procedure used in section IIC was followed for the tail antenna. Fig. 15(a) shows the printed tail antenna on a photo paper and Fig. 15(b), the origami crane after the paper is folded up.  $S_{11}$  of less than -10 dB at both 2.4 GHz and 5.2 GHz bands compares well to that of the simulation as shown in Fig. 16 for flap angle  $\alpha$  of  $90^\circ$ . Fig. 17 shows simulated and measured antenna radiation pattern at (a) 2.4 GHz and (b) 5.2 GHz bands. Both planes  $xy$  and  $yz$  have nulls in the  $y$ -axis while plane  $xz$  indicates omnidirectional radiation. There are differences between the measured and the simulated radiation pattern. This could be due to the small ground plane and the introduction of RF connector/cable to the antenna which affects the current distribution in the ground plane. This changes the impedance and radiation performance. This results in the measured results being slightly different from the simulated results and potentially can make the design validation difficult.

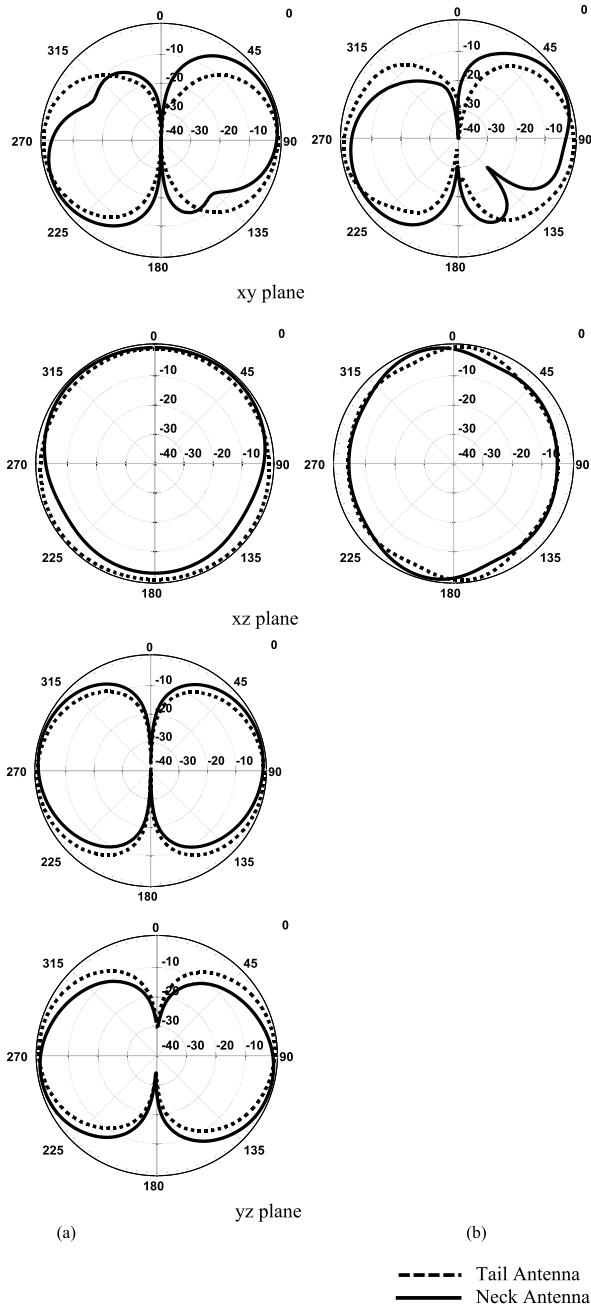


FIGURE 21. Simulated diversity antenna radiation pattern for planes xy, xz, and yz at (a) 2.4 GHz and (b) 5.2 GHz.

Fig. 18 shows the measured and simulated gain versus frequency response at the two frequency bands of interest (2.4-2.5 GHz and 5.0-5.9 GHz). The measured gains are in general lower than simulation ones. The measured gains were about 1.5 dBi at 2.4 GHz and about 2.5 dBi at 5.2 GHz.

#### IV. DIVERSITY ANTENNA SYSTEM SOLUTION

##### A. DIVERSITY ANTENNA SYSTEM DESIGN

Antenna diversity enables improvement of radio communication and enhances the probability of a signal from a transmitter reaching a receiver in a dynamic environment [42] by reducing signal fading, increasing the coverage of the communication system etc.

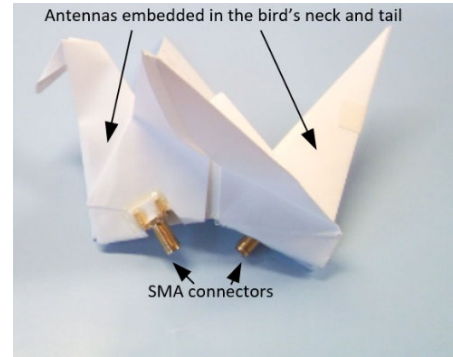


FIGURE 22. Fabricated diversity antenna.

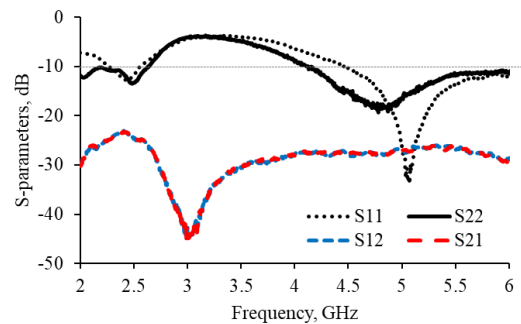
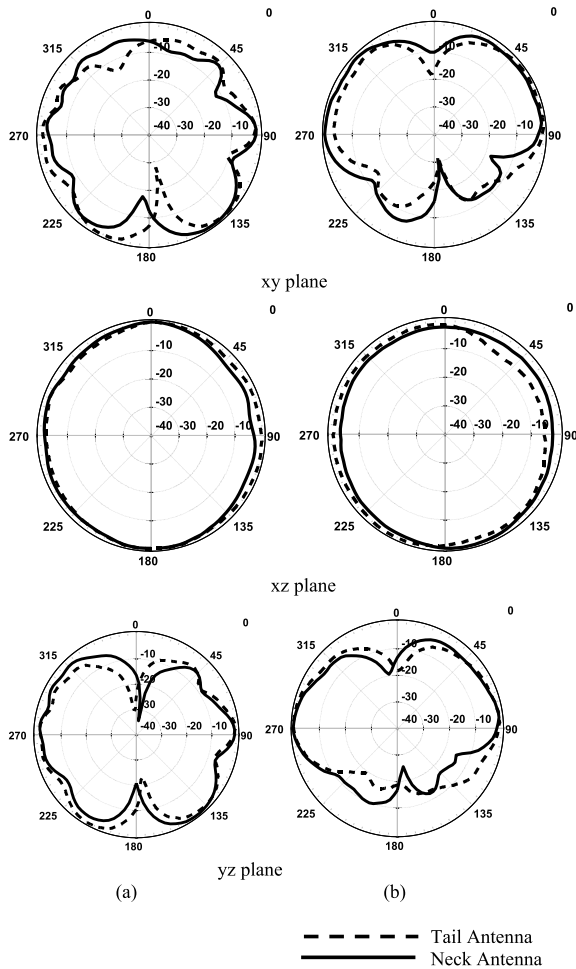


FIGURE 23. Measured diversity antenna S-parameters.

A diversity antenna was created on the neck of the crane, as illustrated in Fig. 19 and also rotated to fit the neck orientation. Each antenna requires an independent RF circuitry and electronics connection and ability to communicate with the control station. The S-parameters i.e.  $S_{11}$ ,  $S_{12}$ ,  $S_{21}$  and  $S_{22}$  of the simulated model were obtained and are shown in Fig. 20.  $S_{11}$  curve is slightly different from  $S_{22}$  curve. This is due to the robot's wings extending over the front antenna and acting as an extra layer of substrate.  $S_{11}$  of  $-10$  dB impedance bandwidths from 2.36 GHz to 2.55 GHz at the lower band and 5.07 GHz to 6 GHz at the higher band respectively were realized.  $S_{22}$  of  $-10$  dB impedance bandwidths from 2.27 GHz to 2.50 GHz and 5.11 GHz to 6 GHz at lower and upper bands respectively were realized.  $S_{12}$  and  $S_{21}$  of less than  $-10$  dB at the resonance frequencies indicates a good antenna isolation between the two antennas. Simulated diversity antennas co-polarization radiation patterns are shown in Fig. 21 (a) at 2.4 GHz and (b) at 5.2 GHz bands for planes xy, xz and yz for the tail and neck antenna. The radiation pattern indicates nulls about the y-axis for xy and yz planes and an omnidirectional radiation pattern for the xz plane for both the tail and neck antennas at both bands. There is improvement in coverage in all planes compared to just one antenna on the tail. The radiation patterns of the two antennas are generally in the same direction that could be due to the two antennas being similarly orientated.

##### B. FABRICATION AND MEASUREMENT

The diversity antennas were fabricated, Fig. 22, as per the procedure described in section 11C. A VNA was used to



**FIGURE 24.** Measured diversity antenna radiation patterns for planes *xy*, *xz* and *yz* at (a) 2.4 GHz and (b) 5.2 GHz.

measure the S-parameters whose plots are shown in Fig. 23. An  $S_{11} - 10\text{dB}$  impedance bandwidth from 2.3 GHz to 2.55 GHz at the lower band and 4.5 GHz to 6 GHz at the upper band respectively was achieved for a flap angle  $\alpha$  of  $90^\circ$ . An  $S_{22} - 10\text{ dB}$  bandwidth from 2.2 GHz to 2.65 GHz at the lower band and 4.3 GHz to 6 GHz the upper band respectively was also realized.  $S_{12}$  and  $S_{21}$  of less than  $-23\text{ dB}$  at both 2.4 GHz and 5.2 GHz bands indicates good isolation between the two antennas.

The orientation of the axis for the measurement of the radiation pattern of the neck is symmetrically to that for the tail. Fig. 24 depicts the measured radiation patterns of planes *xy*, *xz* and *yz* respectively at (a) 2.4 GHz and (b) 5.2 GHz for the two antennas. It indicates nulls in the *xy* and *yz* planes and omnidirection in the *xz* plane for two frequency bands which is commensurate with simulation results. As expected, the radiation patterns for the two antennas are similar. Improvement in coverage is expected when connected to a diversity antenna system.

Table 4 compares previous dual bands WLAN inkjet printed antennas with the one proposed in this work. It can be seen that with comparable gain and bandwidth, the proposed antenna is relatively small in size and is the only one

**TABLE 3.** Comparison between the proposed antenna and previous WLAN Inkjet printed antennas.

Reference	Freq. (GHz)	Bandwidth (GHz)	Gain (dB)	Substrate	Size (mm <sup>3</sup> )
[19]	2.4	1.12	-7.2	NinjaFlex	65×54×1.2
[43]	2.45	0.77	1.81	PET	45×40×0.14
	5.8	2.91	3.92		
[45]	2.4	0.9	3.74	Paper	54×57×0.18
	5.8	2.9	4.96		
This work	2.4	0.45	1.40	Paper	51×34×0.18
	5.2	1.60	2.78		

specifically designed to fit the space available in the origami flapping crane.

### V. DISCUSSION AND CONCLUSION

The integration of inkjet printed planar monopole antennas on an origami flapping robot has been demonstrated. A wideband monopole antenna consisting of a semi-elliptical shape with a triangular part and a horizontal slot has been developed and tested. The dimensions of the triangular section determine resonance at 2.4 GHz while the dimensions of the semi-elliptical section determine resonance at the 5.2 GHz band, the unlicensed frequency bands for drones' control.

The antenna fits on the available space on the traditional origami structure and is able to operate at the required bands. Two optimal solutions were achieved: one on the spine and the other on tail and/or neck.

A diversity system involving the tail and neck antennas was also realized. This increases coverage in a communication system. All the antennas exhibited nearly omnidirectional radiation pattern in the XZ planes at both frequency bands making them suitable for the purpose. The monopole antennas have been fabricated on standard photo paper substrate. A chemical sintering-based silver nanoparticle conductive ink cartridge was used to print the antennas using an inexpensive and ordinary home inkjet printer and photo paper. This made fabrication of the antenna cheap and fast. The successful outcome promises the potential of integration of antennas with flexible electronic systems using inkjet printing technology.

This holds out prospects of appropriation of instant printing technology for fast integration of antenna and flexible electronic systems on paper substrate for future wireless controlled aerial robots in line with [45]. This promises potential realization of other electronics components on a paper substrate as well as potential realization of fully integrated expendable robot.

### ACKNOWLEDGMENT

The authors would like to thank Simon Jakes and Antonio Mendoza for their help in fabrication and measurements, and Dr. Zhijiao Chen for the useful comments.

### REFERENCES

[1] M. Siegel, "Smart sensors and small robots," in *Proc. IMTC 18th IEEE Instrum. Meas. Technol. Conf. Rediscovering Meas. Age Informat.*, May 2001, pp. 303–308.

- [2] J. Huddleston, "The use of small robots for laboratory manipulations," *J. Phys. E, Sci. Instrum.*, vol. 18, no. 11, pp. 891–896, Nov. 1985.
- [3] J. W. Simatupang and M. Yosua, "A remote controlled car using wireless technology," *J. Electr. Electron. Eng.*, vol. 1, no. 2, pp. 56–61, 2016.
- [4] H. J. Kim, D. H. Shim, and S. Sastry, "Flying robots: Modeling, control and decision making," in *Proc. IEEE Int. Conf. Robot. Autom.*, May 2002, pp. 66–71.
- [5] M. Bualat, J. Barlow, T. Fong, C. Provencher, and T. Smith, "Astrobee: Developing a free-flying robot for the international space station," in *Proc. AIAA SPACE Conf. Expo.*, Aug. 2015, p. 4643.
- [6] H. Shigemune, S. Maeda, Y. Hara, N. Hosoya, and S. Hashimoto, "Origami robot: A self-folding paper robot with an electrothermal actuator created by printing," *IEEE/ASME Trans. Mechatronics*, vol. 21, no. 6, pp. 2747–2754, Jul. 2016.
- [7] E. A. P. Hernandez, D. J. Hart, and D. C. Lagoudas, "Design and simulation of origami structures with smooth folds," *Proc. Roy. Soc. A, Math., Phys. Eng. Sci.*, vol. A473, Apr. 2017, Art. no. 20160716.
- [8] Z. Song, T. Ma, R. Tang, Q. Cheng, X. Wang, D. Krishnaraju, R. Panat, C. K. Chan, H. Yu, and H. Jiang, "Origami lithium-ion batteries," *Nature Commun.*, vol. 5, p. 3140, Jan. 2014.
- [9] S. Miyashita, S. Guitron, M. Ludersdorfer, C. R. Sung, and D. Rus, "An untethered miniature origami robot that self-folds, walks, swims, and degrades," in *Proc. IEEE Int. Conf. Robot. Autom. (ICRA)*, May 2015, pp. 1490–1496.
- [10] Y. A. Nijssure, G. Kaddoum, N. Khaddaj Mallat, G. Gagnon, and F. Gagnon, "Cognitive chaotic UWB-MIMO detect-avoid radar for autonomous UAV navigation," *IEEE Trans. Intell. Transp. Syst.*, vol. 17, no. 11, pp. 3121–3131, Nov. 2016.
- [11] C. Liu, G. Wang, Y. Yan, C. Bao, Y. Sun, and D. Fan, "Pint-sized military UAV engine's tele-adjusting arm based on force feedback," in *Proc. 2nd Int. Asia Conf. Informat. Control, Autom. Robot. (CAR)*, Mar. 2010, pp. 205–209.
- [12] P. J. Singh and R. de Silva, "Design and implementation of an experimental UAV network," in *Proc. Int. Conf. Inf. Commun. Technol. (ICOICT)*, Mar. 2018, pp. 168–173.
- [13] D.-G. Kang and J. Choi, "Compact segmented loop antenna for UAV applications," in *Proc. Int. Symp. Antennas Propag. (ISAP)*, Oct. 2017, pp. 1–2.
- [14] V. Camarchia, A. Chiolerio, M. Cotto, J. Fang, G. Ghione, P. Pandolfi, M. Pirola, R. Quaglia, and C. Ramella, "Assessment of silver nanoparticle inkjet-printed microstrip lines for RF and microwave applications," in *Proc. IEEE Int. Wireless Symp. (IWS)*, Apr. 2013, pp. 1–4.
- [15] J. Heirons, S. Jun, A. Shastri, B. Sanz-Izquierdo, D. Bird, L. Winchester, L. Evans, and A. McClelland, "Inkjet printed GPS antenna on a 3D printed substrate using low-cost machines," in *Proc. Loughborough Antennas Propag. Conf. (LAPC)*, Nov. 2016, pp. 1–4.
- [16] S. Jun, B. Sanz-Izquierdo, and M. Summerfield, "UWB antenna on 3D printed flexible substrate and foot phantom," in *Proc. Loughborough Antennas Propag. Conf. (LAPC)*, Nov. 2015, pp. 1–5.
- [17] D. Unnikrishnan, D. Kaddour, S. Tedjini, E. Bihar, and M. Saadaoui, "CPW-fed inkjet printed UWB antenna on ABS-PC for integration in molded interconnect devices technology," *IEEE Antennas Wireless Propag. Lett.*, vol. 14, pp. 1125–1128, 2015.
- [18] S. F. Jilani and A. Alomainy, "An inkjet-printed MMW frequency-reconfigurable antenna on a flexible PET substrate for 5G wireless systems," in *Proc. Loughborough Antennas Propag. Conf. (LAPC)*, Nov. 2017, pp. 1–3.
- [19] M. Rizwan, M. W. A. Khan, L. Sydanheimo, J. Virkki, and L. Ukkonen, "Flexible and stretchable brush-painted wearable antenna on a three-dimensional (3-D) printed substrate," *IEEE Antennas Wireless Propag. Lett.*, vol. 16, pp. 3108–3112, 2017.
- [20] G. W. Whittow, A. Chauraya, J. C. Vardaxoglou, Y. Li, R. Torah, K. Yang, S. Beeby, and J. Tudor, "Inkjet-printed microstrip patch antennas realization textile for wearable applications," *IEEE Antennas Wireless Propag. Lett.*, vol. 13, pp. 71–73, 2014.
- [21] Y. Al-Naiemy, T. A. Elwi, H. R. Khaleel, and H. Al-Rizzo, "A systematic approach for the design, fabrication, and testing of microstrip antennas using inkjet printing technology," *ISRN Commun. Netw.*, vol. 2012, pp. 1–11, May 2012.
- [22] D. E. Anagnostou, "Organic paper-based antennas," in *Innovation in Wearable and Flexible Antennas*. Southampton, U.K.: WIT Press, 2014, ch. 2, pp. 25–57.
- [23] A. M. Mansour, N. Shehata, B. M. Hamza, and M. R. M. Rizk, "Efficient design of flexible and low cost paper-based inkjet-printed antenna," *Int. J. Antennas Propag.*, vol. 2015, pp. 1–6, Sep. 2015.
- [24] G. Shaker, S. Safavi-Naeini, N. Sangary, and M. M. Tentzeris, "Inkjet printing of ultrawideband (UWB) antennas on paper-based substrates," *IEEE Antennas Wireless Propag. Lett.*, vol. 10, pp. 111–114, 2011.
- [25] B. S. Cook and A. Shamim, "Inkjet printing of novel wideband and high gain antennas on low-cost paper substrate," *IEEE Trans. Antennas Propag.*, vol. 60, no. 9, pp. 4148–4156, Sep. 2012.
- [26] H. A. Elmobarak, S. K. A. Rahim, M. Himdi, X. Castel, and T. A. Rahman, "Low cost instantly printed silver nano ink flexible dual-band antenna onto paper substrate," in *Proc. 11th Eur. Conf. Antennas Propag. (EUCAP)*, Mar. 2017, pp. 3061–3063.
- [27] A. T. Elwi, "A miniaturized folded antenna array for MIMO applications," *Wireless Pers. Commun.*, vol. 98, no. 2, pp. 1871–1883, 2018.
- [28] BBC. *Origami Bird Gets BBC Reporter in a Flap*. Accessed: Mar. 5, 2019. [online]. Available: <https://www.bbc.co.uk/news/av/technology-37568222/origami-bird-gets-bbc-reporter-in-a-flap>
- [29] A. Bolton. *Japanese Electronics Maker Creates Origami-Style Drone*. Accessed: Mar. 5, 2019. [Online]. Available: <https://www.cnet.com/news/helping-an-origami-crane-fly-with-a-little-help-from-some-modern-technology/>
- [30] J. Romeu, A. Aguiasca, J. Alonso, S. Blanch, and R. R. Martins, "Small UAV radiocommunication channel characterization," in *Proc. 4th EuCAP*, Apr. 2010, pp. 1–5.
- [31] J. Chen, K.-F. Tong, and J. Wang, "A triple band arc-shaped slot patch antenna for UAV GPS/Wi-Fi applications," in *Proc. Int. Symp. Antennas Propag. (ISAP)*, vol. 1, pp. 367–370, 2013.
- [32] N. P. Agrawal, G. Kumar, and K. P. Ray, "Wide-band planar monopole antennas," *IEEE Trans. Antennas Propag.*, vol. 46, no. 2, pp. 294–295, Feb. 1998.
- [33] G. Kumar and K. P. Ray, *Broadband Microstrip Antennas*. Norwood, MA, USA: Artech House, 2003.
- [34] C.-H. Hsu, "Planar multilateral disc monopole antenna for UWB application," *Microw. Opt. Technol. Lett.*, vol. 49, no. 5, pp. 1101–1103, 2007.
- [35] A. C. Balanis, *Antenna Theory Analysis and Design*, 3rd ed. Hoboken, NJ, USA: Wiley, 2005.
- [36] Z. N. Chen, T. S. P. See, and X. Qing, "Small printed ultrawideband antenna with reduced ground plane effect," *IEEE Trans. Antennas Propag.*, vol. 55, no. 2, pp. 383–388, Feb. 2007.
- [37] M. E. de Cos and F. Las-Heras, "Polypropylene-based dual-band CPW-fed monopole antenna [Antenna applications Corner]," *IEEE Antennas Propag. Mag.*, vol. 55, no. 3, pp. 264–273, Jun. 2013.
- [38] Y. Kawahara, S. Hodges, B. S. Cook, C. Zhang, and G. D. Abowd, "Instant inkjet circuits: Lab-based inkjet printing to support rapid prototyping of UbiComp devices," in *Proc. ACM Int. Joint Conf. Pervas. Ubiquitous Comput. UbiComp*, 2013, pp. 363–372.
- [39] *AGICAN01 Silver Nano Ink, AGICCP01A4 Special Coated Paper*, AgIC, Tokyo, Japan, 2014.
- [40] Z. N. Chen, M. J. Ammann, X. Qing, X. H. Wu, T. S. See, and A. Cai, "Planar antennas," *IEEE Microw. Mag.*, vol. 7, no. 6, pp. 63–73, Dec. 2006.
- [41] K. S. Ryu and A. A. Kishk, "UWB dielectric resonator antenna having consistent omnidirectional pattern and low cross-polarization characteristics," *IEEE Trans. Antennas Propag.*, vol. 59, no. 4, pp. 1403–1408, Jan. 2011.
- [42] S. Johnsrud and S. Hellan, "Antenna diversity," Texas Instruments Incorporate, Dallas, TX, USA, Appl. Rep. SWRA469, 2014.
- [43] M. M. Bait-Suwailam and A. Alomainy, "Flexible analytical curve-based dual-band antenna for wireless body area networks," *Prog. Electromagn. Res. M*, vol. 84, pp. 73–84, 2019.
- [44] S. Jun, J. Heirons, and B. Sanz-Izquierdo, "Inkjet printed dual band antenna for paper UAVs," in *Proc. 11th Eur. Conf. Antennas Propag. (EUCAP)*, Mar. 2017, pp. 3452–3456.
- [45] G. Grau, E. J. Frazier, and V. Subramanian, "Printed unmanned aerial vehicles using paper-based electroactive polymer actuators and organic ion gel transistors," *Microsyst. Nanoeng.*, vol. 2, no. 1, pp. 1–8, Dec. 2016.



**PETER M. NJOGU** is currently pursuing the Ph.D. degree in electronic engineering with the School of Engineering and Digital Arts, University of Kent, Canterbury, U.K. His research interests include wearable antennas, multiband antennas, and 3-D printed antennas.



**BENITO SANZ-IZQUIERDO** (Member, IEEE) received the B.Sc. degree from ULPGC, Spain, and the M.Sc. and Ph.D. degrees from the University of Kent, U.K.

He was a Research Associate with the School of Engineering, University of Kent, in 2013, where he became a Lecturer in electronic systems and, in 2018, a Senior Lecturer. In 2012, he has worked for Harada Industries Ltd., where he developed novel antennas for the automotive industry. His research interests include multiband antennas, wearable electronics, additive manufacturing (3D printing), substrate integrated waveguides components, metamaterials, electromagnetic band-gap structures, frequency selective surfaces, and reconfigurable devices.

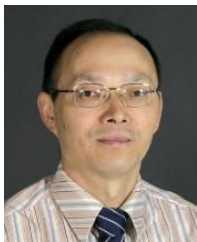
Dr. Sanz-Izquierdo has received awards and recognition for his work on wearable antennas (mention in the House of Lords, the IEEE IWAT Best Paper Award), frequency selective surfaces (the Best Paper at the IET Workshop on Aerospace Applications Award), and reconfigurable antennas (the 2017 CST University Publication Award for the IEEE TRANSACTIONS paper). His research has been funded through a variety of sources, such as the U.K. EPSRC, the Royal Academy of Engineering, and the Royal Society.



**SUNG YUN JUN** (Member, IEEE) received the M.S. degree in electrical engineering from Syracuse University, USA, in 2008, and the Ph.D. degree from the University of Kent, U.K., in 2018. Since December 2018, he has been a Postdoctoral Researcher with the National Institute of Standards and Technology, Boulder, CO, USA. His current research interests include antenna design, millimeter-wave channel measurements, and modeling of radio propagation.



**GABRIEL KALMAN** graduated as an Electronics and Communications Engineer from the University of Kent. He is currently working for an American telecommunication company called CommScope Technologies fulfilling a Reliability and Test Engineer position. This position involves operating and managing the dedicated test center, for qualifications and validations on CommScope microwave systems antennas encapsulating any reliability test.



**STEVEN (SHICHANG) GAO** (Fellow, IEEE) received the Ph.D. degree from Shanghai University, China, in 1999.

He is currently a Professor and the Chair of RF and microwave engineering, and the Director of Postgraduate Research with the School of Engineering and Digital Arts, University of Kent, U.K. His research interests include smart antenna, phased array, MIMO, broadband and multi-band antennas, small antennas, RF/microwave/mm-wave circuits, RF front ends, FSS, and their applications into 5G mobile communications, satellite communication, small satellites, radars, energy harvesting, and medical systems. He co-edited/coauthored

three books, including the *Space Antenna Handbook* (Wiley, 2012), the *Circularly Polarized Antennas* (Wiley-IEEE, 2014), and the *Low-Cost Smart Antennas* (Wiley, 2019); over 300 articles; and eight patents. He is a Fellow of the Royal Aeronautical Society and the IET. He received the 2016 IET Premium Award for the Best Paper in *IET Microwaves, Antennas and Propagation* and the 2017 CST University Publication Award for a paper in the IEEE TRANSACTIONS ON ANTENNAS AND PROPAGATION. He was a Distinguished Lecturer of the IEEE Antennas and Propagation Society, from 2014 to 2016. He was an Invited Speaker in many international conferences (Plenary Speaker at AES'2014, Invited Speaker at IWAT'2017, UCMAT'2017, IWAT'2014, SOMIRES'2013, and APCAP'2014). He was the General Chair of the 2013 Loughborough Antenna and Propagation Conference, U.K. He is an Associate Editor of five Journals such as the IEEE TRANSACTIONS ON ANTENNAS AND PROPAGATION, *Radio Science*, *Electronics Letters*, IEEE ACCESS, and *IET Circuits, Devices and Systems*; the Editor-in-Chief of *Microwave and Wireless Technologies* (Wiley Book Series); and an Editorial Board Member of many international Journals. He was a Guest Editor of the Special Issue on "Photonic and RF Communications Systems" of the *IET Circuits, Devices and Systems* in 2014, the Special Issue on "Antennas for Satellite Communication" of the *IEEE Transactions on Antennas and Propagation* in 2015, and the Special Issue on "Small Satellites" of the PROCEEDINGS OF THE IEEE in March 2018.



**ASISH MALAS** received the Ph.D. degree in materials science (polymer) from IIT Kharagpur, India, in 2014.

He is currently a Researcher with the PolyMERIC-LSBU Innovation Centre, TWI Ltd., Cambridge, U.K. His research interests include additive manufacturing and 3d printing of polymers/composites, processing and fabrication of polymer composites/nanocomposites, polymer rheology (flow), conducting and dielectric polymers/composites, nanoparticles (Graphene, and CNTs), and material characterizations.



**GREGORY J. GIBBONS** received the Ph.D. degree from the Department of Physics, University of Warwick. After time spent in the private sector, he returned to Warwick to join WMG, in 1997, where he has been the Head of the Additive Manufacturing (AM) Group, since 2001, providing excellence in research, teaching, and knowledge transfer of AM and related technologies. His research interests include new applications for AM and development of next-generation AM technologies.

He was appointed as a Reader at WMG, in 2014. He has over 20 years' experience in the field of AM, with more than 60 peer reviewed publications, H-index 12. He has a wide portfolio of funded research, being a Principal Investigator on a number of EPSRC, IUK, HVM Catapult, and industrially funded projects, including collaborations with U.K. and EU Universities, Research Organizations, and industry. His strong industrial engagement extends from SMEs through to OEMS (e.g., BAE Systems, Bombardier, Unilever, and AkzoNobel). He is a long standing Fellow of the Institute of Materials, Minerals and Mining and the Co-Chair of the High Value Manufacturing Catapult AM Forum, promoting AM across the HVM Centers to industry.

...